Structural and electronic properties of *p*-doped silicon clathrates

D. Connétable*

*Laboratoire de Physique de la Matière Condensée et des Nanostructures, Bâtiment Brillouin, 43 Bd du 11 Novembre 1918,
Université Claude Bernard Lyon I and CNRS, 69622 Villeurbanne, France*

We present an *ab initio* study of the structural and electronic properties of type-I and type-II silicon clathrates doped by elements chosen to be more electronegative than silicon. Depending on the intercalated element, we show that the electronic properties of doped silicon clathrates can exhibit metallic, semiconducting, or insulating behavior. It is found in particular that doping can lead to silicon-based materials with a band gap in the visible range and that, in type-II clathrates, the gap can be direct. However, the analysis of the selection rules show that the optical transitions are forbidden in type-I and type-II clathrates. Concerning the structural properties, the bonding between the dopant atom and silicon can significantly decrease the compressibility of the host network to values equivalent to the one of the much denser diamond phase. The present results are complemented and rationalized by the study of endohedrally doped Si_nH_n ($n=20, 24, 28$) silicon clusters.

I. INTRODUCTION

Four decades after their first synthesis by Kasper *et al.*,[1] clathrates have recently attracted new attention from both experimentalists and theoreticians due to their promising structural, electronic, dynamical, and superconducting properties. This can be related, in particular, to the discovery of a BCS superconductivity at $T \sim 8$ K in Ba_xNa_y@Si-46 clathrates.[2–4] Theoretical predictions[5–15] that the band gap in empty silicon clathrates is ~ 0.7 eV larger than the one of the silicon diamond phase have been confirmed experimentally,[16] thus providing novel perspectives in optoelectronic applications. The low compressibility of such phases,[17–19] the high stability under pressure,[17] the prospect of using clathrates as low work function materials,[20] the prediction of more generally efficiently doped semiconducting phases,[21] and the high thermoelectric power of doped clathrates[22–25] are other subjects of current research. Further, due to a rapid progress in the techniques of synthesis, new types of clathrates are constantly appearing. For example, systems containing such doping atoms as alkali metals, alkaline earth metals, or noble metals and frameworks made of combinations of Cu, Al, Ga, In in substitution of Si, Ge, or Sn have been synthesized.

Clathrates are cagelike open framework compounds, composed of three-dimensional networks of polyhedra which are sharing faces. Nearest neighbor distances and angles between the bonds are approximately the same as those we find in the diamond phase [in the silicon case $d(Si-Si) \approx 2.35 \pm 0.05$ Å, $\Theta(Si-Si) \approx 109 \pm 5°$], and all atoms are also linked together through sp^3-type covalent bonds. The presence of 87% of pentagonal cycle (contrary to the diamond phase where there are only hexagonal cycles) is expected to be at the origin of the specific electronic and dynamical properties of clathrates.[14]

Clathrates are mainly classified into two types. The type-I clathrate, called Si-46, crystallizes in a simple cubic (sc) lattice with 46 atoms per unit cell and a $Pm\bar{3}n$ (No. 223) symmetry. We distinguish two sorts of cages in the network: 2 dodecahedral (12-hedral with 12 pentagonal cycles) X_{20} cages ($X=Si, Ge, Sn$) of I_h point symmetry, and 6 tetrakaidecahedra X_{24} (14-hedral with 12 pentagonal and 2 opposing hexagonal cycles) cages of D_{6d} symmetry, which are connected together by sharing their faces [see Fig. 1(a)]. The type-II clathrate Si-34 (often referred to as Si-136) is a face centered cubic (fcc) lattice with 34 atoms in the unit cell and a $Fd\bar{3}m$ (No. 227) symmetry. This crystal can be seen as an aggregate of 2 hexadecahedral (16-hedral with 12 pentagonal and 4 hexagonal cycles) X_{28} cages (T_d) [Fig. 1(b)] at each site of the fcc unit cell. The space between the 16-hedral cages forms other cages of (4) 12-hedral X_{20}.

The originality of such structures is the possibility of a high endohedral doping, that is doping by inserting (intercalation) until there is one atom in each cage (which corresponds to 20% of doping). From this point of view, doping of clathrates is much easier than doping of the diamond phase. As it will be shown later, intercalation can lead to dramatic changes of the electronic and structural properties. In a previous work,[26] we reported our theoretical results on the unusual structural and electronic properties of I_8@Si-46 clathrate synthesized recently by Reny *et al.*[27] In the present paper, we expand our study and report our *ab initio* results for Si-46 and Si-34 clathrates doped by seven elements (Xe,
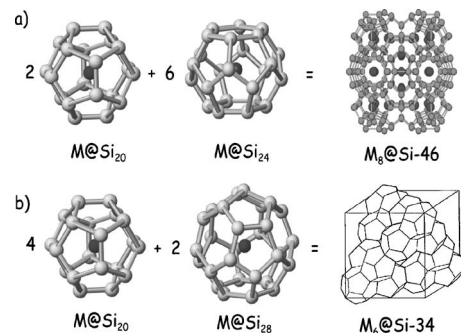

FIG. 1. Symbolic ball-and-stick representation of the composition of (a) M_8@Si-46: six 14-hedral Si_{24} cages and two 12-hedral Si_{20} cages and (b) M_6@Si-34 clathrates: two 16-hedral Si_{28} cages and four 12-hedral Si_{20} cages.

I, Te, Sn, Kr, Br, and Ge) from the right side of the periodic table. We have not explored all the possibilities of intercalation, however we would like to give a general overview of this type of doping. The variety of doping elements will allow us to perform a comparative analysis and to predict and to understand the evolution of the interaction of the doping element with the host network. As a result, the evolution of the properties of the material can be further analyzed.

The paper is organized as follows. In Sec. II, we briefly outline our computational framework. In Sec. III A, we present first-principle calculations on type-I clathrate doped by the elements mentioned above. To understand the origin of the modification of the electronic properties under doping, we study, in Sec. III B, the isolated clusters $Si_{20}H_{20}$, $Si_{24}H_{24}$, and $Si_{28}H_{28}$ doped by the same elements. We focus in particular on the role of symmetries in driving the electronic properties. Such a symmetry (group theory) analysis is extended to the clathrate phase in the Sec. III C. To confirm our results, we have also performed first-principles calculations of Kr_8@Si-46 and Br_8@Si-46 in Sec. III D, Xe_6@Si-34 and I_6@Si-34 clathrates in Sec. III E. Finally, we conclude this paper with the study in Sec. III F of the optical transitions in empty and Xe-doped Si-46 and Si-34 clathrates at high symmetry points of the Brillouin zone.

II. COMPUTATIONAL DETAILS

Our calculations were done within the density functional theory[28,29] (DFT) in the local density approximation (LDA). The Perdew-Zunger parametrization[30] of the Ceperley-Alder homogeneous electron gas exchange-correlation potential[31] was used. The valence electrons were treated explicitly while the influence of the core electrons and atomic nuclei was replaced by norm-conserving Trouiller-Martins pseudopotentials[32] factorized in Kleinman-Bylander form.[33] For the doping elements, pseudopotentials were generated including scalar relativistic effects and a nonlinear core correction[34] was used to mimic some of the effects of the d shell on the valence electrons.

We employed the SIESTA program package[35] which is a self-consistent pseudopotential code based on numerical pseudoatomic orbitals (PAOs) as the basis set for decomposition of the one-electron wave functions. A well-converged basis set, consisting of doubled $\{s, p_x, p_y, p_z\}$ orbitals plus polarization d-orbitals was adopted. The charge density was calculated on a real-space grid with a spacing equivalent to 80 Ryd cutoff. For structure optimization, the Brillouin Zone (BZ) was sampled by a $2 \times 2 \times 2$ Monkhorst and Pack grid[36] which corresponds to 1 and 2 irreducible **k** points for M_8@Si-46 (sc lattice) and M_6@Si-34 (fcc lattice) clathrates respectively. For the calculation of the density of states, we have adopted a fine $8 \times 8 \times 8$ grid (20 and 60 irreducible **k** points, respectively).

All systems studied below were fully relaxed both with respect to the unit cell size and atomic positions. To evaluate the bulk modulus, several structural relaxations for different unit cell volumes were performed, and the results were fitted by a Murnaghan equation of state.[37]

TABLE I. Calculated bulk modulus (GPa), binding energy (eV), formation energy (in eV per M element) and lattice parameter a_0(Å) for M_8@Si-46 ($M=$Xe, I, Te, Sn, Kr, Br, and Ge) and for M_6@Si-34 (where $M=$Xe and I) clathrates. A negative binding energy means that the M element is not binding inside the cages (see text). The bulk modulus of Si-2 is calculated to be 97 GPa.

M element	Si-46	Sn	Te	I	Xe
$B_{0\ (theory)}$	87	97	95	91	85
$E_{binding}$		3.3	3.1	1.7	−0.6
E_f		−1.1		0.65	
a_0	10.05	10.04	10.06	10.13	10.23
M element		Ge		Br	Kr
$B_{0\ (theory)}$		97		92	87
$E_{binding}$		3.0		0.7	−0.5
E_f		−1.1			
a_0		9.97		10.08	10.17
M element	Si-34			I	Xe
$B_{0\ (theory)}$	86			90	84
$E_{binding}$				1.65	−0.63
E_f				0.60	
a_0	14.53			14.64	14.75

III. RESULTS AND DISCUSSION

A. The case of the $(Xe \rightarrow Sn)_8$@Si-46 clathrates

Calculated structural parameters and cohesive energies for type-I silicon clathrates are presented in Table I. Seven elements of the periodic table ($M=$Xe, I, Te, Sn, Kr, Br, and Ge) were chosen as possible dopants. The stoichiometry of the calculated structures was M_8@Si-46, i.e., both Si_{24} and Si_{20} cages were filled with the doping elements M. We restrict our choice by placing the doping element at the center of the cages. In this section, we concentrate on the compounds where the doping elements belong to the fifth row of the periodic table (Xe, I, Te, Sn). Such a work has been suggested by the recent synthesis of I- and Te-doped clathrates.[27,38,39]

We first discuss the structural and mechanical properties of the systems under study and in particular their binding energies $E_{binding}(M)=\frac{1}{8}[E(Si46)+8E(M)-E(M_8@Si46)]$. We take as a reference the energy of the undoped Si-46 clathrate, and the isolated atom[40] of the doping element. The results (Table I) suggest that all elements, except for the noble gas (Xe and Kr), are stabilized by being intercalated inside the Si-46 network. In particular, we find that I atom prefers to sit in the middle of the silicon cages rather than in I_2 dimers (by 0.65 eV atom), which is consistent with the experimental fact that I_8@Si-46 has been already synthesized. On the contrary, in the case of Sn (or Ge) doped element, atom seems prefer to not form doped clathrates (see note Ref. 41): the formation energy (E_f in Table I), taking as references Si-46 and the standard states for Sn (and Ge), is found negative. We will show later, that the increase of the binding energy when going from I to Sn can nevertheless be correlated to the increase of the covalent character of the chemical bond between the dopant and the network.
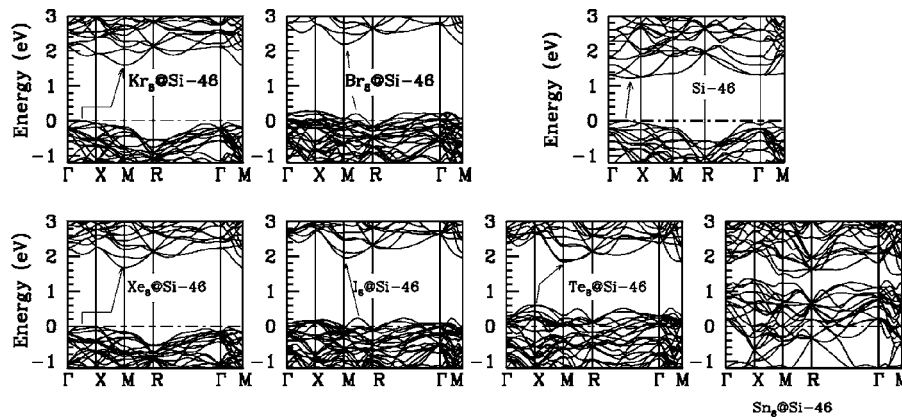
FIG. 2. DFT-LDA band structure of Si-46 and M_8@Si-46 clathrates (M=Xe,I,Te,Sn,Kr,Br) along high symmetry directions of the Brillouin zone. Energies are in eV. The zero of energy has been set to the top of the valence bands for semiconductors and to the Fermi level for metallic systems. The arrows indicate the nature of the band gap.

Concerning the structural properties, it can be clearly seen (Table I) that the lattice parameter is continuously decreasing from Xe to Sn. The unit cell volume of Sn_8@Si-46 system is 5% smaller than that of Xe_8@Si-46, and is even smaller than the unit cell volume of the empty Si-46 structure. On the contrary, standard atomic tables show that the size of the doping atom increases from Xe to Sn. This allows us to conclude that a simple analysis in term of steric (or volume excluded) effects is not appropriate for these systems. Table I also indicates that the lattice contraction is accompanied by a constant increase of the bulk modulus. While being 85 GPa for the Xe_8@Si-46 system, it reaches the value of 97 GPa for Sn_8@Si-46, a value comparable with the bulk modulus of the silicon diamond phase.[42] The high compressibility of Xe doped clathrate rules out the simple idea that a big intercalated atom should necessarily prevent the easy compression of the cages.

Two antagonist effects could explain these main results: the steric effects, due to the confinement of the doped element which expand cages, and the ionic/covalent effects, which contract cages, and characterize the interaction between the network and the doping element. Later, we shall try to analyze the role of both of these effects, and will try to use this analysis to understand our structural data.

We now discuss the electronic structure of the M_8@Si-46 (M=Xe,I,Te,Sn) clathrates. Figure 2 shows the LDA band structure of doped Si-46 clathrates along high symmetry directions of the Brillouin zone. The band structure for undoped Si-46 clathrate is also presented as a reference. As emphasized in the Introduction, the comparison of the band structures clearly indicates that a large variety of electronic properties can be obtained by changing the intercalated atom.

We first focus on the Xe-doped system. Even though the negative binding energy, obtained for the intercalation of rare gas atom, questions the possibilities of synthesizing such a compound, Xe_8@Si-46 will serve us as a useful reference system to study the effect of doping. The most important result is the opening of the band gap (1.65 eV DFT value), which is 0.45 eV larger than that of the empty Si-46 clathrate and 1.1 eV larger than the one of Si-2 diamond (within the

same DFT formalism). Comparing the band structures of Si-46 and Xe_8@Si-46 systems, we observe that the top of the valence bands is hardly modified while the bottom of the conduction bands changes dramatically. Figure 3 presents calculated electronic density of states (*e*DOS) projected onto atomic orbitals for the Xe_8@Si-46 system. The contribution of Xe-5p orbitals is located in the middle of the valence band, while Xe-5s orbitals are located at much lower energy. Peaks A and B belong to 5s orbitals of Xe atoms located inside Si_{20} and Si_{24} cages, respectively. Peak A is always lower in energy, due to the smaller size of the Si_{20} cage. We observe that, in spite of a small Xe weight both at the top of the valence band and at the bottom of the conduction band, the intercalation of Xe atoms modifies strongly the conduction bands of the Si-46 system. Using the symmetry analysis of the character of Si-46 states, we shall show later that the coupling between Xe and Si-46 states takes place at the bottom of the conduction bands thus opening the band gap.

Now we analyze the electronic structure of I_8@Si-46 and Te_8@Si-46 clathrates and compare it with that of the Xe_8@Si-46 system. Contrary to the Xe case, intercalation of I or Te leads to a strong modification of the top valence bands of the silicon network (Fig. 2), which now has a substantial contribution of the guest atoms 5p orbitals (Fig. 3). This is related to the ionic character of the I-Si and Te-Si bonds [using the Pauling scale, the electronegativities of Si, Te, and I are, respectively, 1.90, 2.10, and 2.66 (Ref. 43)]. As a results, charge is transfered to the 5p levels of I and Te which are pushed up to the Fermi level. The integrated *e*DOS for the Iodine system shows that there are exactly four states between the Fermi level and the bottom of the gap, which corresponds exactly to eight I-5p electrons missing in the unit cell. The same integration for Te gives eight states, corresponding to sixteen Te-5p electrons missing. As a result, I and Te systems become *p*-type degenerated doped semiconductors, with the Fermi level located, respectively, 0.26 and 0.68 eV below the "top of the valence band." While the upper valence bands are strongly modified as compared to Xe_8@Si-46, we emphasize that the lower conduction bands are on the contrary very similar. Further, the band gap of I_8@Si-46 is found to be ≈1.6 eV, which is relatively close
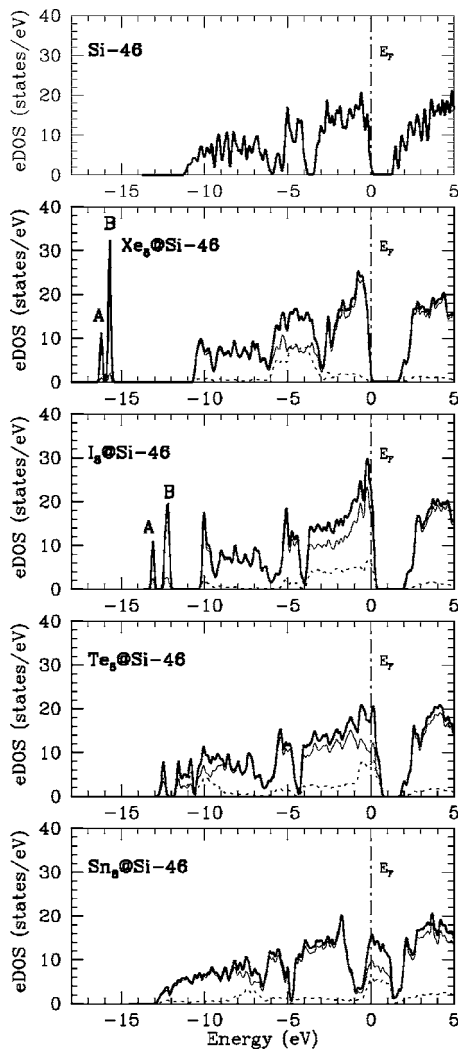
FIG. 3. Electronic density of states (eDOS) for Si-46 and M_8@Si-46 clathrates (M=Xe,I,Te,Sn). Energies are in eV and eDOS in states/eV. The zero of energy has been set to the Fermi level. The thick lines correspond to the total eDOS, the dotted lines correspond to the total eDOS projected on the guest atom orbitals, and the thin lines correspond to the silicon network total eDOS contribution. A 0.1 eV broadening has been used. Peaks A and B represent the s-orbital contribution of the guest atom, located in Si_{20} and Si_{24} cages, respectively.

to the one of Xe$_8$@Si-46 ($\sim$1.65 eV). This indicates that the band gap opening is not related to charge transfer, ionic effects are not indeed expected to occur when doping by Xe. We shall discuss the origin of such a large band gap in the Sec. III C.

We finally studied the evolution of the electronic structure of M@Si-46 clathrates going from M=I to M=Sn. Figure 3 shows that Sn-$5p$ states are now located in the band gap of the empty Si-46, and the doped clathrate becomes a pure metallic system. The reduction of the electronegativity while going from I to Sn (1.96 in Pauling units for Sn[43]) suggests the increase of the covalent part of the chemical bonding between the intercalated atom and the silicon network. This could be a reason for the observed lattice contraction, and the increase of the bulk modulus as it was mentioned above.
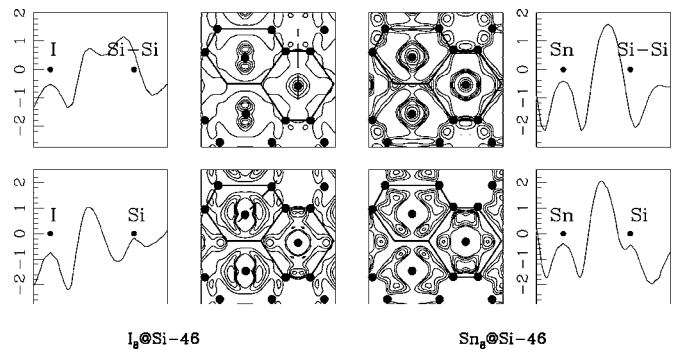

FIG. 4. Contour maps of the $\Delta\rho$ electron density distribution for I$_8$@Si-46 and Sn$_8$@Si-46 clathrates in the (100) plane. $\Delta\rho$ = $\rho(M_8$@ Si-46)-ρ(Si-46)-8*$\rho(M)$ (see text). Each map has been delimited by five levels. The upper figures represents the negative part of the electron density contribution, while the bottom figures represent the positive part. The black circles show the positions of the atoms in the plane. There are five contours (positive or negative) for each map. The extrema correspond, respectively, to −4.5 to +1.6 10^{-3} electron/(a.u.)^3 and −2.2 to +2.0 10^{-3} electron/(a.u.)^3 for I- and Sn-doped clathrates. The black lines between the black circles symbolize the trace of the cages in the planes. We plot also the radial density distribution along two directions. Upper graphs represent it along a M atom and the middle of the bond Si-Si. Bottom figures represent it along a line between M and one atom of the Si$_{24}$ cage. The scale is in 10^{-3} electron/(a.u.)^3.

The nature of the chemical bond can be understood by analyzing the electron density distribution maps. Namely, we calculated the difference between the electronic density of the doped clathrate and a superposition of the electronic density of empty Si-46 (using the same volume) and corresponding "isolated" dopants. The results for the (100) plane are presented in Fig. 4. The positive (bottom) and negative (top) parts of the electronic density are plotted separately for a convenient analysis. The radial electronic density has been plotted for further information along two different directions (dotted lines on the map of the Fig. 4): the first along one Si and M atoms in a Si$_{24}$ cage (bottom), and the second along the middle of a Si-Si bond and M in a Si$_{20}$ cage (top). We notice a charge transfer from the cages to the interstitial space atom for the I- and Sn-doped clathrate. In the case of Sn doping we can clearly see a charge transfer from both the Si network and the doping atom to the space between Si and Sn, which proves our statement about the covalent nature of chemical bonding in this compound. In the case of the I doping there are two effects which we need to take to account, to explain the electronic map: the electronic transfer due to the doping and the extension of the orbitals.

The formation of bonds between Si atoms and the dopant element means that the effective coordination number of Si becomes larger than four. As such, doped Si clathrates can be considered as high density phases of Si at ambient pressures. Their increased coordination numbers may explain why Sn$_8$@Si-46 shows a large bulk modulus combined with a strong metallic character.

At the end of this section we should mention that our results for the band gap opening have been confirmed by accurate many-body calculations within the *GW* approxima-

TABLE II. Binding energy (eV) for $M@Si_xH_x$ ($M=Xe, I$, and $x=20,24,28$) cluster.

Cluster	$Si_{20}H_{20}$	$Si_{24}H_{24}$	$Si_{28}H_{28}$
I	2.4	1.9	1.8
Xe	−0.7	0.0	0.3

tion, performed for the $Xe_8@Si$-46 system.[26,44] The band gap was also found to be 0.6 eV larger as compared to the empty Si-46 clathrate, and twice higher than the silicon diamond phase (gap$_{exp}$=1.15 eV). However, as shown later, the mechanisms responsible for this striking effect can be easily understood within usual DFT-LDA approach, taking into account symmetry considerations.

B. Isolated clusters

For better understanding of the influence of cage-dopant interactions on the electronic properties of type-I and -II clathrates, we have studied the influence of intercalation on isolated hydrogenated clusters the elementary brick of clathrates. The Si_{20}, Si_{24}, and Si_{28} cages were "extracted" from the bulk and all dangling bonds on the cluster surfaces were passivate with hydrogen atoms (to mimic the fourfold coordination as in the clathrate phase). We used unit cells large enough to eliminate the interaction between clusters (the distance between the clusters was more than 20 Å). The clusters were then relaxed with respect to atomic positions without imposing any symmetry limitations.

The case of isolated and intercalated Si cages (H passivated or not) have been studied in the past in order to propose new "building blocks" for designing cluster-made materials (see Refs. 45–47, for example). We study in the following only the intercalated cages which are relevant for our study of the clathrates.

The results show that $Si_{20}H_{20}$ (symmetry I_h), $Si_{24}H_{24}$ (D_{6d}), and $Si_{28}H_{28}$ (T_d) clusters remain stable under I doping as in the clathrate bulk. The symmetry groups of the empty clusters were also well preserved after the relaxation process. This fact allowed us to perform a classification of molecular levels of the clusters according to irreducible representations of the corresponding point group. For the I-doped clusters a small distortion of the cage geometry due to a Jahn-Teller effect was observed. The corresponding splitting of the highest occupied molecular orbital level was found to be about 0.15 eV in $Si_{20}H_{20}$. In the case of Xe doping, the binding energy is negative (non bonding) for $Si_{20}H_{20}$, and positive for $Si_{24}H_{24}$ and $Si_{28}H_{28}$ clusters (see Table II).

Table III presents the energies of four molecular orbitals, including the highest occupied molecular orbital (HOMO) and the lowest unoccupied molecular orbital (LUMO), for each of the clusters. The corresponding irreducible representations are also presented for each of the orbitals. The introduction of the guest atom leads to the shift of the LUMO level to higher energies, yielding an increase of the molecular gap by 0.5 to 0.8 eV (Table III). On the contrary, the HOMO states seem to be hardly affected by the intercalation in the case of $Xe@Si_nH_n$. This effect can be clearly seen on

TABLE III. Energy levels of $Si_{20}H_{20}$, $Si_{24}H_{24}$, and $Si_{28}H_{28}$ clusters near the molecular gap. The symmetry groups of the clusters as well as corresponding IRs of the molecular levels are also presented (see text). The bottom of the table shows the opening of the molecular gap due to intercalation, and the IRs of the corresponding guest atom orbitals in the crystal field of the cluster. The reference energy has been set to the HOMO level.

	$Si_{20}H_{20}$ (I_h)	$Si_{24}H_{24}$ (D_{6d})	$Si_{28}H_{28}$ (T_d)
Mol. Lev.	E (eV)	E (eV)	E (eV)
HOMO−1	−0.3 (G_u)	−0.2 (E_4)	−0.1 (E)
HOMO	0.0 (H_u)	0.0 (B_1)	0.0 (T_1)
LUMO	+2.9 (A_g)	+2.8 (A_1)	+2.9 (A_1)
LUMO+1	+3.6 (T_{1u})	+3.4 (E_1)	+3.5 (T_2)
Molecular gap opening due to intercalation (eV)			
IR	(T_{1u}, A_g)	(B_2, E_1, A_1)	(T_2, A_1)
I	1.0	0.6	0.5
Xe	0.9	0.6	0.5

presented eDOS for $Si_{20}H_{20}$ clusters with Xe and I doping (Fig. 5). The results are comparable to those obtained for the bulk clathrate phase.

This result is at first sight somewhat counterintuitive, as the $5p$ shell of Xe or I lies below the HOMO levels. The standard repulsion by hybridization mechanism between two levels (see Fig. 6) would call for a closing of the gap by repulsion of the HOMO level. However, as shown previously for Xe-doped systems, the top of the valence bands (and the HOMO states of the clusters) are hardly modified by the intercalation. To understand this fact we shall concentrate on
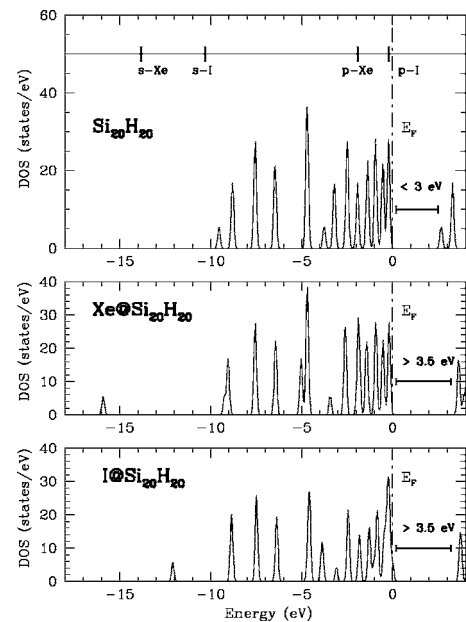
FIG. 5. Electronic density of states (states/eV) for $Si_{20}H_{20}$, $Xe@Si_{20}H_{20}$, and $I@Si_{20}H_{20}$ clusters. The upper panel also shows the position of s and p orbitals of free Xe and I atoms.
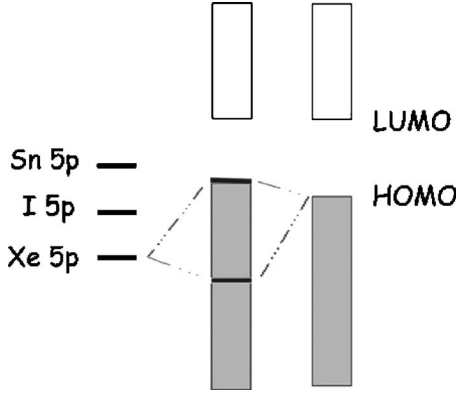
FIG. 6. Schematic representation of the expected coupling of the guest 5p orbitals with the HOMO level of the silicon clathrate or cluster. On the right, the position of the Xe, I, and Sn levels with respect to the top of the valence bands of clathrate is provided.

the results presented in Table III and try to find out the reason for the increase of the molecular gap. The molecular field of the cluster causes the splitting of s and p orbitals of the guest atom into several irreducible representations, depending on the point symmetry group of the cluster. Let us consider as an example the $Si_{20}H_{20}$ cluster. The symmetry group of the cluster is I_h, and the orbitals of the guest atom split into the following irreducible representations (IRs): $A_g \oplus T_{1u}$. We see that these representations are present in the IRs of two lowest unoccupied molecular orbitals, but can not be found among IRs of two highest occupied orbitals. This shows that only the lowest unoccupied orbitals can couple with the orbitals of the guest atom, while coupling with the highest occupied states is forbidden by symmetry. As a result, only the LUMO states are "repelled" by the intercalated orbitals. This mechanism leads to the increasing of the molecular gap value, as observed on eDOS plots (Fig. 5). Exactly the same effect is observed for $Si_{24}H_{24}$ and $Si_{28}H_{28}$ clusters (Table III). The described hybridization is stronger for smaller cages, leading to a larger gap for the $Si_{20}H_{20}$ cluster.[48]

C. Symmetry analysis in the clathrate phase

Now keeping in mind all our results obtained for the clusters, we turn back to clathrates and apply the same type of symmetry analysis for the bulk phase. We have analyzed the symmetries of five bands (three valence and two conduction) at three **k** points of the irreducible part of the BZ. We took the **Γ** point, the middle between the **Γ** and **X** points, and the middle between **X** and **M** points (see Fig. 2). For each **k** point and each energy band, we determined the irreducible representation (IR) of the respective point group. The results for Si-46 and Xe_8@Si-46 systems are summarized in Table IV.

First, we consider the high-symmetry **Γ** point. The doping atoms are located at positions with point group O_h, and the crystal field causes the splitting of s and p orbitals of the doping atom into the following irreducible representations:

$$IR_s = [A_{1g} \oplus A_{2g}] \oplus [A_{1g} \oplus E_g \oplus T_{2u}] \text{ and}$$

TABLE IV. Symmetry classification of the valence and conduction bands near the fundamental gap for Si-46 and Xe_8@Si-46 systems (simple cubic lattice). The energies are calculated at three **k** points of the Brillouin zone. The **k** points along the **Γ-X** (Δ) and **X-M** (**Z**) directions are taken in the middle of the corresponding intervals. The bottom of the table shows the IRs of the momentum operator for the corresponding **k**-points, and the possibility of a direct dipole transition. The reference energy has been set to top of the valence bands.

	Si-46		
	Γ (O_h)	Δ (C_{4v})	**Z** (C_{2v})
Band	E (eV)	E (eV)	E (eV)
E_{v3}	−0.24 (E_u)	−0.26 (E)	−0.33 (B_2)
E_{v2}	−0.23 (T_{2g})	−0.19 (B_2)	−0.20 (A_2)
E_{v1}	−0.13 (A_{1u})	0.00 (A_2)	−0.15 (A_2)
E_{c1}	+1.32 (T_{1u})	+1.23 (A_1)	+1.30 (A_1)
E_{c2}	+1.59 (A_{2g})	+1.45 (B_1)	+1.45 (B_1)
	Xe_8@Si-46		
E_{v3}	−0.29 (T_{1g})	−0.17 (E)	−0.33 (B_2)
E_{v2}	−0.28 (E_u)	−0.08 (B_2)	−0.20 (A_2)
E_{v1}	−0.21 (T_{2g})	0.00 (A_2)	−0.15 (A_2)
E_{c1}	+2.15 (E_g)	+2.14 (B_1)	+2.30 (A_1)
E_{c2}	+2.32 (A_{2g})	+2.24 (B_1)	+2.45 (B_1)
	Irreductible representation of **p**		
	Γ (O_h)	Δ (C_{4v})	**Z** (C_{2v})
	T_{1u}	$E+A_1$	$A_1+B_1+B_2$
	Optical transitions		
Si-46	no	no	no
Xe_8@Si-46	no	no	no

$$IR_p = [\underline{T_{1u}} \oplus T_{2u}] \oplus [\underline{2T_{1u}} \oplus T_{2u} \oplus E_g \oplus A_{2g} \oplus T_{1g} \oplus T_{2g}],$$

where the IRs for the atom in the Si_{20} (Si_{24}) cages. are given on the left (right) of the $\oplus$ direct product.

We observe that the top of the valence band and the bottom of the conduction band belong to A_{1u} and T_{1u} representation respectively. However, only T_{1u} representation is present among the IRs of the doping atom. This leads to the conclusion that only the bottom of the conduction bands can couple to the orbitals of the guest atom, leading to the band gap opening. This is similar to what was observed in the case of isolated clusters. As the T_{1u} representation is present among IRs of the p orbitals of the doping atoms located both in Si_{20} and Si_{24} cages, both intercalation sites should contribute to the change of the band structure.[49] There exists of course certain states in the valence band which are allowed to interact with the orbitals of the guest atom. As a result of interaction, these states are also pushed to higher energies (Table IV), but this shift is not large enough to enter in the band gap (Fig. 2).
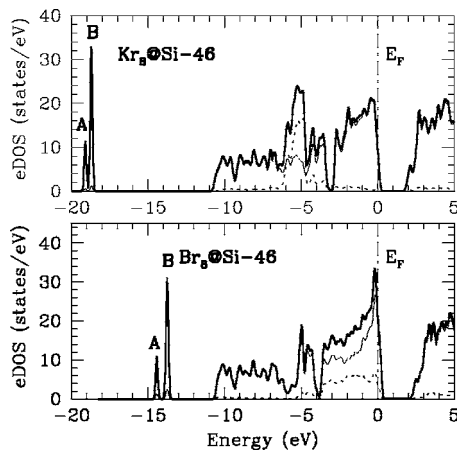
FIG. 7. Electronic density of states (eDOS) for Kr_8@Si-46 and Br_8@Si-46 clathrates. The same notations as in Fig. 3 are used.

D. Electronic and structural properties of Si-46 clathrates doped by Kr, Br, and Ge

It is interesting to see if the results obtained above for doping elements in the Xe row, remain valid in the Kr serie. We have therefore performed calculations of type-I clathrates doped by three elements from the fourth row of the periodic table. We studied Kr_8@Si-46, Br_8@Si-46, and Ge_8@Si-46 systems. The calculated lattice parameter, bulk modulus and binding energy for each of the systems are presented in Table I. Comparing these results with the data obtained for the fifth row elements studied before (Table I), we observe exactly the same behavior. The bulk modulus continuously increases and reaches 97 GPa for the Ge-doped system, while the unit cell contracts to a volume smaller than the volume of the empty Si-46 structure.

The band structure (Fig. 2) and the electronic density of states (Fig. 7) also shows a strong similarity between Xe_8@Si-46 and Kr_8@Si-46 systems, as well as between I_8@Si-46 and Br_8@Si-46 systems. Xe- and Kr-doped clathrates remain pure semiconductors, while I- and Br-doped systems become p-type doped semiconductors. The hybridization of the conduction band states with the orbitals of the guest atom leads to the increasing of the band gap value, which becomes larger than 2 eV for Br_8@Si-46 system (DFT value). This is even larger than what was obtained for elements in the Xe line. Nothing prevents to believe that even larger gap values may be achieved.

E. Electronic and structural properties of Xe- and I-doped Si-34 clathrates

To make our research complete, we have explored the effect of Xe and I doping on atomic and electronic structure of type-II clathrates. This study will provide us with additional information to check the trends observed in the previous section. At the same time, the results obtained for the isolated clusters indicated that Si_{20} cages have stronger influence on the electronic properties of the doped clathrates than Si_{28} cages. The study of type-II clathrate will give us a possibility to check the validity of this statement.

Table I presents the calculated structural characteristics and binding energies for Xe_6@Si-34 and I_6@Si-34 clathrates. The same characteristics for the empty Si-34 structure are also presented for sake of comparison. We see that the structural parameters exhibit the same tendency as in the Si-46 structure. Going from Xe to I, we observe an increase of the bulk modulus accompanied by a decrease of the lattice parameter.

The calculated binding energies for type-I clathrates show that the I atom prefers to sit inside the clathrate cages, while Xe atom does not. However, the calculation of Si-34 systems where Xe is located in Si_{28} or in Si_{20} only cages yields binding energies of ~ 0 and ~ -1.6 eV respectively. This demonstrates that Si_{28} cages are the first candidates to be occupied by the guest atoms even when this doping is energetically unfavorable. This correlates with the experimental results of Reny *et al.*,[50] who observed that sodium atoms prefer to sit in Si_{28} cages in the Na_x@Si-34 compound.

We first focus on Xe-doped clathrate Xe_6@Si-34. The most important result (Fig. 8) is again a large direct (≈ 1.95 eV DFT value) band gap, as compared to 1.30 eV for the empty Si-34 clathrate. As in the case of Xe_8@Si-46, we notice that the bottom of the conduction band is strongly modified under doping while the top of the valence band is only slightly modified. As we shall see later, the symmetry considerations can help us to understand this effect. For I_6@Si-34, we also obtain a p-type semiconductor behavior, with three states between the Fermi level and the top of the valence band. This corresponds, as in the I_8@Si-46 case, exactly to the number of states to fill the I shell. In the two doped type-II clathrates, we observe a direct band gap at the **L** point, exactly as in the empty Si-34 system.

To clarify the influence of different cages on the electronic properties of the compound, we performed additional calculations of Xe_2@Si-34 and Xe_4@Si-34 structures with Xe atoms in Si_{28} and Si_{20} cages only, respectively. The calculations were performed taking the atomic coordinates of Xe_6@Si-34 system without structure relaxation and any modifications of the unit cell (the difference between these unrelaxed systems and the corresponding relaxed one is small). Figure 8 shows the band structure of these systems. We observe a negligible modification of the band structure of Si-34 after intercalating a guest atom in the Si_{28} cages. On the contrary, the modifications are substantial after the Si_{20} cages are filled with the doping element. For both Xe_2@Si-34 and Xe_4@Si-34 systems we calculated the difference between the electronic density of the doped system and a superposition of the electronic density of empty Si-34 and Xe atoms (not represented here). For the Xe_2@Si-34 structure, we hardly observe any influence of the doping atom, which is clearly not the case for the Xe_4@Si-34 structure. These results demonstrate the fundamental role of Si_{20} cages in the formation of the electronic structure of the doped clathrate systems.[51]

To check that the hybridization mechanisms between the guest atom and the host network are the same for type-I and type-II clathrates, we perform a symmetry analysis for doped Si-34 system at the Γ point. The s and p orbitals of the guest atom split to the following irreducible representations: $IR_s = [A_{2u} \oplus A_{1g}] \oplus [A_{1g} \oplus T_{2g}]$ and $IR_p = [T_{2g} \oplus T_{1u}] \oplus [A_{2u}$
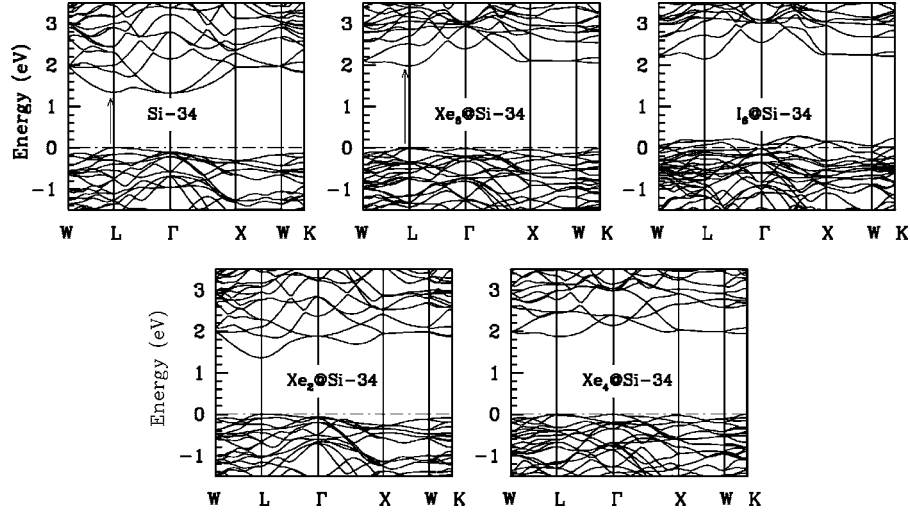
FIG. 8. DFT-LDA band structure of Si-34, Xe$_6$@Si-34, and I$_6$@Si-34 clathrates along high symmetry directions of the Brillouin zone. We add the band structure of Xe$_2$@Si-34, and Xe$_4$@Si-34 systems, obtained taking the unit cell size and atomic coordinates of Xe$_6$@Si-34, without additional relaxation (see text).

$\oplus 2T_{1u} \oplus E_u \oplus T_{2u}$], where the IRs for the atom in the Si$_{20}$ (Si$_{28}$) cages. are given on the left (right) of the $\oplus$ direct product.

Table V presents the energies of three valence and two conduction bands of Si-34 structure with their respective irreducible representations. We see that the top of the valence bands and the bottom of the conduction bands belong to T_{1g} and T_{1u} representations, respectively. However, only the T_{1u} representation can be found among IRs of the doping element. This shows that the coupling takes place mostly with the bottom of the conduction bands, leading to the band gap opening. We see that the hybridization mechanism is exactly the same as we observed while studying Si-46 structure and the cluster models.

F. Optical transitions

The present study demonstrates that contrary to the Si-46 clathrate, the Si-34 structure shows a direct band gap which can be as large as 2 eV (DFT value) under Xe or I doping (Fig. 8). This value is probably even larger ($\sim$2.6 eV) if we accept the assumption that the GW correction of 0.6 eV is the same for type-I and type-II clathrates.[26] The direct nature of the band gap and its large value calls for possible use of doped clathrate in optoelectronic devices. This invited us to study the optical transitions in Si-34 and Si-46 systems.

This study can be performed using two different approaches. First of all, the momentum matrix elements $\langle \Psi_{n\mathbf{k}} | \mathbf{P} | \Psi_{n'\mathbf{k}} \rangle$ can be directly calculated numerically for all band combinations and each $\mathbf{k}$ point. Another method is to find irreducible representations of the momentum operator $\mathbf{P}$ and one-electron wave functions $\Psi_{n\mathbf{k}}$ and $\Psi_{n'\mathbf{k}}$. The selection rules[52] can be further applied to determine if a transition is possible or not. We used a symmetry-based approach, although the first method was also used in parallel in several cases to make sure that both approaches give exactly the same results.

Tables IV and V present the irreducible representations of the one-electron states near the band gap as well as the IRs for the momentum operator for {Si-46, Xe$_8$@Si-46} and {Si-34, Xe$_6$@Si-34} structures, respectively. For Si-46 clathrates,

TABLE V. Symmetry classification of the valence and conduction bands near the fundamental gap for Si-34 and Xe$_6$@Si-34 systems (fcc lattice). The energies are calculated at four $\mathbf{k}$ points of the BZ. The points in L-Γ (Λ) and Γ-X (Δ) directions are taken close to **L** and **Γ** points, respectively. The bottom of the table shows the IRs of the momentum operator for corresponding $\mathbf{k}$ points, and the possibility of a direct dipole transition.

	L (D_{3d})	Λ (C_{3v})	Γ (O_h)
	Si-34		
Band	E (eV)	E (eV)	E (eV)
E_{v3}	-0.30 (E_u)	-0.31 (E)	-0.21 (T_{2u})
E_{v2}	-0.17 (E_g)	-0.16 (E)	-0.12 (E_u)
E_{v1}	0.00 (A_{2g})	-0.05 (A_2)	-0.11 (T_{1g})
E_{c1}	1.30 (A_{1g})	$+1.31$ (A_1)	$+1.30$ (T_{1u})
E_{c2}	1.79 (A_{1g})	$+1.77$ (A_1)	$+2.11$ (A_{2u})
	Xe$_6$@Si-34		
E_{v3}	-0.34 (E_u)	-0.39 (E)	-0.23 (T_{1g})
E_{v2}	-0.04 (A_{2g})	-0.09 (A_2)	-0.21 (T_{2u})
E_{v1}	0.00 (E_g)	-0.02 (E)	-0.03 (E_u)
E_{c1}	$+1.95$ (A_{1g})	$+2.02$ (A_1)	$+2.33$ (A_{2u})
E_{c2}	$+2.46$ (A_{2u})	$+2.41$ (A_1)	$+2.92$ (T_{2g})
	Irreducible representation of **p**		
	L (D_{3d})	Λ (C_{3v})	Γ (O_h)
	$A_{2u}+E_u$	$E+A_1$	T_{1u}
	Optic transition?		
Si-34	no	no	no
Xe$_6$@Si-34	no	yes	no

the study was performed at the high-symmetry Γ point, as well as along Γ-**X** and **X**-**M** directions (Δ and **Z** directions, respectively). We see that the direct electric-dipole transitions are not allowed by symmetry in Si-46 system in the chosen **k** points and directions. The situation is not changed by intercalation, although, as it was pointed out before, the conduction bands change dramatically.

For Si-34 systems, the study was performed at all high symmetry points and directions of the Brillouin zone. Table V shows the results only for Γ and **L** points and along the **L**-Γ and Γ-**X** directions (respectively, Λ and Δ directions). The band structure of Si-34 predicts a direct transition at the high-symmetry **L** point (Fig. 2). However, the symmetry analysis shows that the electric-dipole transition is not allowed at this point, neither for the undoped Si-34, nor for Xe-doped structure. The transition is also forbidden in all the other high-symmetry **k** points of the BZ for both systems. We found that for the undoped Si-34 case, the direct transitions are allowed only along the Γ-**X** direction. These transitions are also allowed for the Xe-doped structure, but the change of the bands topology near the gap allows additional direct transitions along the **L**-Γ direction (Table V).

At first sight, such results does not play in favor of using doped clathrate in opto-electronic applications, even though the switching of the dipole matrix elements along the **L**-Γ direction for $Xe_6@Si$-34 means that at finite temperature a few electrons would be allowed to relax by emitting a visible light photons. However, a more complete study of doping by other elements or of stress induced symmetry breaking would be interesting to see if the dipole matrix elements can be made non zero. Our results can be compared with those of the type-III clathrate (hex-Si-40) presented by Galvani *et al.*[21] They have shown that this latter clathrate (hypothetical phase) shows too a direct but nonactive optical transition.

IV. CONCLUSION

We have reported an extensive *ab initio* study of structural and electronic properties of type-I and type-II silicon clathrates doped by the elements more electronegative than silicon. We have released a general behavior of the doping by elements more electronegative than silicon. It was demonstrated that physical and mechanical properties of silicon clathrates can be tuned in a wide range by choosing an appropriate dopant from the right side of the periodic table. In particular, doping by the noble gas atoms increases significantly the band gaps of Si-46 and Si-34 systems (up to 1.9 eV DFT value). Doping by I, Te, or Br atoms (moving to the left in the periodic table) leads to the formation of a *p*-type doped semiconductor with the gap up to 2 eV. And, finally, doping by Sn or Ge atoms makes a pure metallic system out of type-I and type-II clathrates. Our results show that the hybridization mechanisms between the electronic states of the guest atom and the host network play a fundamental role in increasing the bulk modulus and opening of the fundamental gap of silicon clathrates. Using a group theoretical analysis, we have further demonstrated that in Si-46 and Si-34 clathrates the orbitals of the guest atom couple mostly with the bottom of the conduction band of the silicon network, while coupling with the top of the valence band is forbidden by symmetry. These mechanisms were verified by studying doped Si_{20}, Si_{24}, and Si_{28} clusters—the building blocks of the clathrates. Finally, we have demonstrated that the symmetry of the system influences significantly the optical properties of Si-46 and Si-34 clathrates. In particular, a direct optical transition, which was predicted by *ab initio* calculations for Si-34 clathrate, appears to be forbidden by symmetry in a dipole approximation.

ACKNOWLEDGMENTS

*Present address: CIRIMAT-ENSIACET, 118 route de Narbonne, 31077 Toulouse, France. Electronic address: Damien.Connetable@ensiacet.fr

[1] J. S. Kasper, P. Hagenmuller, M. Pouchard, and C. Cros, Science **150**, 1713 (1965); C. Cros, M. Pouchard, P. Hagenmuller, and J. S. Kasper, Bull. Soc. Chim. Fr. **7**, 570 (1970); C. Cros, M. Pouchard, and P. Hagenmuller, J. Solid State Chem. **2**, 570 (1970); C. Cros, M. Pouchard, and P. Hagenmuller, Bull. Soc. Chim. Fr. **2**, 379 (1971).

[2] H. Kawaji, H. O. Horie, S. Yamanaka, and M. Ishikawa, Phys. Rev. Lett. **74**, 1427 (1995).

[3] K. Tanigaki, T. Shimizu, K. M. Itoh, J. Teraoka, Y. Moritomo, and S. Yamanaka, Nat. Mater. **2**, 653 (2003).

[4] D. Connétable, V. Timoshevskii, B. Masenelli, J. Beille, J. Marcus, B. Barbara, A. M. Saitta, G.-M. Rignanese, P. Mélinon, S. Yamanaka, and X. Blase, Phys. Rev. Lett. **91**, 247001 (2003).

[5] G. B. Adams, M. O'Keeffe, A. A. Demkov, O. F. Sankey, and Y.-M. Huang, Phys. Rev. B **49**, 8048 (1994).

[6] A. Kitano, K. Moriguchi, M. Yonemura, S. Munetoh, A. Shintani, H. Fukuoka, S. Yamanaka, E. Nishibori, M. Takata, and M. Sakata, Phys. Rev. B **64**, 045206 (2001).

[7] S. Yamanaka, E. Enishi, H. Fukuoka, and M. Yasukawa, Inorg. Chem. **39**, 56 (2000).

[8] J. D. Bryan, V. I. Srdanov, G. D. Stucky, and D. Schmidt, Phys. Rev. B **60**, 3064 (1999).

[9] K. Moriguchi, M. Yonemura, A. Shintani, and S. Yamanaka, Phys. Rev. B **61**, 9859 (2000).

[10] A. A. Demkov, O. F. Sankey, K. E. Schmidt, G. B. Adams, and M. O'Keeffe, Phys. Rev. B **50**, 17001 (1994).

[11] S. Saito and A. Oshiyama, Phys. Rev. B **51**, R2628 (1995).

[12] V. I. Smelyanski and J. S. Tse, Chem. Phys. Lett. **264**, 459 (1997).

[13] P. Mélinon, P. Kéghélian, X. Blase, J. Le Brusq, A. Perez, E. Reny, C. Cros, and M. Pouchard, Phys. Rev. B **58**, 12590

(1998).

[14] K. Moriguchi, S. Munetoh, and A. Shintani, Phys. Rev. B **62**, 7138 (2000).

[15] A. Moewes, E. Z. Kurmaev, J. S. Tse, M. Geshi, M. J. Ferguson, V. A. Trofimova, and Y. M. Yarmoshenko, Phys. Rev. B **65**, 153106 (2002).

[16] J. Gryko, P. F. McMillan, R. F. Marzke, G. K. Ramachandran, D. Patton, S. K. Deb, and O. F. Sankey, Phys. Rev. B **62**, R7707 (2000).

[17] A. San-Miguel, P. Kéghélian, X. Blase, P. Mélinon, A. Perez, J. P. Itié, A. Polian, E. Reny, C. Cros, and M. Pouchard, Phys. Rev. Lett. **83**, 5290 (1999).

[18] A. SanMiguel, P. Mélinon, D. Connétable, X. Blase, F. Tournus, E. Reny, S. Yamanaka, and J. P. Itié, Phys. Rev. B **65**, 054109 (2002).

[19] J. S. Tse, S. Desgreniers, Z.-Q. Li, M. R. Ferguson, and Y. Kawazoe, Phys. Rev. Lett. **89**, 195507 (2002).

[20] V. Timoshevskii, D. Connétable, and X. Blase, Appl. Phys. Lett. **80**, 1385 (2002).

[21] E. Galvani, G. Onida, S. Serra, and G. Benedek, Phys. Rev. Lett. **77**, 3573 (1996); M. Bernasconi, S. Gaito, and G. Benedek, Phys. Rev. B **61**, 12689 (2000).

[22] J. L. Cohn, G. S. Nolas, V. Fessatidis, T. H. Metcalf, and G. A. Slack, Phys. Rev. Lett. **82**, 779 (1999).

[23] J. S. Tse, K. Uehara, R. Rousseau, A. Ker, C. I. Ratcliffe, M. A. White, and G. MacKay, Phys. Rev. Lett. **85**, 114 (2000).

[24] G. S. Nolas, J.-M. Ward, J. Gryko, L. Qiu, and M. A. White, Phys. Rev. B **64**, 153201 (2001).

[25] L. Qiu, M. A. White, Z. Li, J. S. Tse, C. T. Ratcliffe, C. A. Tulk, J. Dong, and O. F. Sankey, Phys. Rev. B **64**, 024303 (2001).

[26] D. Connétable, V. Timoshevskii, E. Artacho, and X. Blase, Phys. Rev. Lett. **87**, 206405 (2001).

[27] E. Reny, S. Yamanaka, C. Cros, and M. Pouchard, Chem. Commun. (Cambridge) **24**, 2505 (2000).

[28] P. Hohenberg and W. Kohn, Phys. Rev. **136**, B864 (1964).

[29] W. Kohn and L. J. Sham, Phys. Rev. **140**, A1133 (1965).

[30] J. P. Perdew and A. Zunger, Phys. Rev. B **23**, 5048 (1981).

[31] D. M. Ceperley and B. J. Alder, Phys. Rev. Lett. **45**, 566 (1980).

[32] N. Troullier and J. L. Martins, Phys. Rev. B **43**, 1993 (1991).

[33] L. Kleinman and D. M. Bylander, Phys. Rev. Lett. **48**, 1425 (1982).

[34] S. G. Louie, S. Froyen, and M. L. Cohen, Phys. Rev. B **26**, 1738 (1982).

[35] P. Ordejón, E. Artacho, and J. M. Soler, Phys. Rev. B **53**, R10441 (1996); D. Sánchez-Portal, P. Ordejón, E. Artacho, and J. M. Soler, Int. J. Quantum Chem. **85**, 453 (1997).

[36] H. J. Monkhorst and J. D. Pack, Phys. Rev. B **13**, 5188 (1976).

[37] F. D. Murnaghan, Proc. Natl. Acad. Sci. U.S.A. **30**, 244 (1944).

[38] N. Jaussaud, M. Pouchard, G. Goglio, C. Cros, A. Ammar, F. Weill, and P. Gravereau, Solid State Sci. **5**, 1193 (2004).

[39] N. Jaussaud, P. Toulemonde, M. Pouchard, A. San Miguel, P. Gravereau, S. Pechev, G. Goglio, and C. Cros, Solid State Sci. **6**, 401 (2004).

[40] See A. Dal Corso, A. Pasquarello, A. Baldereschi, and R. Car, Phys. Rev. B **53**, 1180 (1996) concerning the spin correction to include in the calculation of the energy of isolated atom.

[41] We have computed the formation energies of the Sn and Ge standard states: β-tin and diamond for Sn (respectively, 4.37, 4.43 eV/atom), and diamond for Ge (4.10 eV/atom). Our results reproduce correctly the lattice parameters and the formation energies already published [see B. H. Cheong and K. J. Chang, Phys. Rev. B **44**, 4103 (1991); N. E. Christensen and M. Methfessel, *ibid.* **48**, 5797 (1993); P. Pavone, S. Baroni, and S. de Gironcoli, *ibid.* **57**, 10421 (1998), for Sn, and M. T. Yin and M. L. Cohen, *ibid.* **24**, 6121 (1981) for Ge].

[42] We pay attention to use the same spacing data points to fit energy in all materials studied. We notice a negligible difference between the simple bulk-modulus directly calculated and including the correction introduced by Rignanese. G. M. Rignanese, P. Ghosez, J. C. Charlier, J. P. Michenaud, and X. Gonze, Phys. Rev. B **52**, 8160 (1995).

[43] www.webelements.com

[44] X. Blase, Phys. Rev. B **67**, 035211 (2003).

[45] V. Kumar and Y. Kawazoe, Phys. Rev. Lett. **90**, 055502 (2003).

[46] F. Pichierri, V. Kumar, and Y. Kawazoe, Chem. Phys. Lett. **383**, 544 (2004).

[47] F. Pichierri, V. Kumar, and Y. Kawazoe, Chem. Phys. Lett. **406**, 341 (2005).

[48] Q. Sun, Q. Wang, T. M. Briere, V. Kumar, Y. Kawazoe, and P. Jena, Phys. Rev. B **65**, 235417 (2002), and the references.

[49] We can notice that, in the clusters, the s orbital of the doped element is coupling with the LUMO, while, in the clathrates, it is the p shells which are coupling.

[50] E. Reny, P. Gravereau, C. Cros, and M. Pouchard, J. Mater. Chem. **8**, 2839 (1998).

[51] In the case of type-I clathrates, Si_{24} cages are not significantly smaller than Si_{20} cages (in particular in the hexagon to hexagon center direction) and the distinction between the role of different cages is not so clear.

[52] P. Y. Yu and M. Cardona, in *Fundamentals of Semiconductors* (Springer-Verlag, Berlin, 1996).